Approximate and exact numerical integration of the gas dynamic equations

Timothy S. Lewis and Lawrence Sirovich

Division of Applied Mathematics

Brown University, Providence, Rhode Island 02912

Report prepared for NASA Langley Research Center under

NASA Grant no. NSG 1617

Abstract

Two-dimensional steady supersonic flow over an airfoil is considered. A highly accurate approximation and a new, rapidly convergent numerical procedure partly based on it are developed. Examples for a symmetric airfoil over a range of Mach numbers are given. Several interesting features are found in the calculation of the tail shock and the flow behind the airfoil.

1. Introduction

This paper contains an investigation of two-dimensional supersonic gas dynamic flows. Although the final step in our investigation is numerical, we use methods which incorporate our analytical and physical know edge of such flows. The approach is well-suited both for numerical integration and for the interpretation of the resulting flow phenomena. In the present investigation, several new or little-known effects concerning the tail shock and flow behind a two-dimensional airfoil emerge. Discussion of these is reserved for section 6. A preliminary version of this approach for the case of one-dimensional unsteady flow has already been reported (Sirovich & Chong 1980, Chong & Sirovich 1980).

For problems in which the shock waves are weak, variations in entropy and one Riemann invariant are third-order effects, and the solution is approximately given by a simple wave, or Prandtl-Meyer expansion (Friedrichs 1948; see Lighthill 1960 for corrections and extensions). In fact the numerical change in the Riemann invariant is significantly smaller than that in entropy (section 3). This suggests that a larger class of flows can be viewed as the interaction of a simple wave and an entropy variation, which in turn suggests that streamlines and principal characteristics be used as coordinates. Adamson (1968) has used a similar coordinate system in another context.

The usefulness of this transformation is also related to shock expansion theory, a method for calculating surface pressures which goes back to Epstein (1931). It depends upon the fact that reflections of the outgoing waves on the principal characteristics are weak and tend to cancel each other (Hayes & Probstein 1966, Mahony 1955). Shock expansion theory has been extended to include computation of the full flow field (Eggers, Syvertson & Kraus 1953, Meyer 1957). Jones (1963), in another approach, bridges shock expansion theory and simple wave theory by considering slowly varying perturbations of the latter. Our approximate solution is closely related to shock expansion theory.

We use the approximate solution as the first step of an iterative numerical method to compute the exact solution. This procedure is quite distinct from current numerical methods for this type of problem. For the most part such approaches apply a variety of differencing schemes to the gas dynamic equations in their standard form (for a comparison of several methods see Taylor, Ndefo & Masson 1972). Implementation is then relatively simple, but may require many mesh points and/or be subject to restrictive stability criteria. Methods which do not explicitly fit shock waves also tend to have difficulty with them, producing oscillations near or diffusing the discontinuity. A more powerful method which fits the shock wave explicitly is the RVLP method (Babenko, et al. 1966, Holt 1979). This is a rather unwieldy method, which is actually intended for

more complicated problems than that dealt with here. The method of characteristics (see Liepmann & Roshko 1957, ch. 12), to which our method is more closely related, has also been found in practice to be unwieldy and time-consuming.

Comparisons of computation time are difficult to make, because of the many variables involved, but the procedure we present should compare favorably with others available. The approximate solution is probably sufficiently accurate in many instances, and even in the worst cases we have calculated only about three or four iterations are required to achieve an accuracy of one percent throughout the flow field.

2. Formulation of problem

We consider the situation shown in figure 1, in which a uniform flow of Mach number $M_0>1$ is incident upon a two-dimensional symmetric airfoil. It is assumed that there are attached shocks at the leading and trailing edges, and that the flow remains supersonic everywhere. We discuss the flow in the upper half plane ahead of the tail shock. The tail shock and the flow behind it are treated in appendix B. If the airfoil is not symmetric, the flow fields above and below it can each be computed by the methods described here, independently, up to the appearance of the tail shocks.

The coordinates x and y are scaled by the airfoil length;

the pressure p and the density ρ by their upstream values p_o and ρ_o; the velocity $(u,v) = (q \cos\theta, q \sin\theta)$ and the sound speed a by the upstream sound speed a_o; and the entropy s, which is set to zero upstream, by the gas constant R. We consider a perfect gas with constant specific heats $c_v = R/(\gamma-1)$ and $c_p = \gamma c_v$, for which the equation of state is $p = \rho^\gamma \exp[(\gamma-1)s]$ and the sound speed is given by $a^2 = p/\rho$. The calculations here were done for $\gamma = 1.4$. Modifications for the case of a gas with a general equation of state are outlined in Appendix A.

The equations of inviscid two-dimensional steady flow are conveniently written in characteristic form with the entropy s, the flow angle θ, and the Mach angle $\mu = \sin^{-1}(1/M)$ (where $M=q/a$ is the local Mach number) as dependent variables. All other physical quantities can be obtained from these and Bernoulli's equation

$$a^2 + \frac{\gamma-1}{2} q^2 = 1 + \frac{\gamma-1}{2} M_o^2. \qquad (1)$$

The equations of motion are (Meyer 1960, p. 273)

$$ds = 0 \quad \text{on streamlines:} \quad \frac{dy}{dx} = \tan\theta, \qquad (2)$$

$$d(\theta+P(\mu)) = \frac{1}{2\gamma} \sin 2\mu \, ds \quad \text{on} \quad C^+: \quad \frac{dy}{dx} = \tan(\theta+\mu), \qquad (3)$$

$$d(\theta - P(\mu)) = -\frac{1}{2\gamma} \sin 2\mu \, ds \quad \text{on} \quad C^-: \frac{dy}{dx} = \tan(\theta - \mu), \tag{4}$$

where $P(\mu)$ is given by

$$P(\mu) = \sqrt{\lambda} \tan^{-1}(\sqrt{\lambda} \tan \mu) - \mu, \qquad \lambda = (\gamma+1)/(\gamma-1).$$

The streamlines and the C^+ and C^- characteristics are shown in figure 1. The quantities $r^{\pm} = \theta \pm P(\mu)$ are called the Riemann invariants. Another useful form of (3) and (4) is

$$d\theta \pm \frac{1}{2\gamma} \sin 2\mu \frac{dp}{p} = 0 \quad \text{on} \quad C^{\pm}: \frac{dy}{dx} = \tan(\theta \pm \mu). \tag{5}$$

The appropriate boundary condition at the airfoil is

$$\tan \theta = f'(x) \quad \text{on} \quad y = f(x). \tag{6}$$

In addition, the solution far away from the airfoil ($y \to \pm\infty$) must approach the upstream conditions $\theta = 0$, $\mu = \mu_o$, and $s = 0$. The jumps in θ, μ, and s across the shocks are governed by the Rankine-Hugoniot conditions (Liepmann & Roshko 1957, p. 85). If we denote the shock angle by η, and flow quantities on either side of the shock by subscripts 1 and 2, these conditions can be written

$$\tan(\theta_2 - \theta_1) = \frac{1}{\tan(\eta - \theta_1)} \frac{(M_1^2 - 1)\tan^2(\eta - \theta_1) - 1}{\left(1 + \frac{\gamma+1}{2} M_1^2\right) + \left(1 + \frac{\gamma-1}{2} M_1^2\right)\tan^2(\eta - \theta_1)}, \tag{7}$$

$$\left(\frac{a_2}{a_1}\right)^2 = (1+z)\,\frac{1+\frac{\gamma-1}{2\gamma}z}{1+\frac{\gamma+1}{2\gamma}z}, \tag{8}$$

$$s_2-s_1 = \frac{1}{\gamma-1}\left[\log(1+z) + \gamma\log\frac{1+\frac{\gamma-1}{2\gamma}z}{1+\frac{\gamma+1}{2\gamma}z}\right], \tag{9}$$

where the shock strength $z = (p_2-p_1)/p_1$ is given by

$$z = \frac{2\gamma}{\gamma+1}\left[M_1^2\sin^2(\eta-\theta_1) - 1\right]. \tag{10}$$

Equation (8) determines the jump in μ, since a^2 can be written as a function of M or μ using (1).

3. A new coordinate system

Across a shock wave the entropy and one of the Riemann invariants (r^- for η positive, r^+ for η negative) change only at third order in the shock strength. This can be shown by Taylor series expansions (or see Courant & Friedrichs 1948, Section 138). In figure 2 the jumps in s and r^- are plotted on a logarithmic scale against the deflection angle θ_2 for various Mach numbers M_1. Without loss of generality we can set $\theta_1=0$ and take θ_2, and hence η,

positive. The shock strength is of the same order as the deflection angle, so for small θ_2, the curves approach straight lines of slope three. For larger values of θ_2, the rates of increase of Δs and Δr^- tend to drop off somewhat.

For a weak shock wave Δs and Δr^- can be considered negligible compared to, say, Δr^+, which is a first-order quantity. These values also provide estimates for the variation in s and r^- throughout the flow field. This is obvious in the case of s, since it is constant on streamlines. In fact the same is very nearly true of r^- for a wide range of conditions. This will be seen in connection with shock expansion theory later on. Therefore, for a weak shock wave s and r^- are nearly constant everywhere, and the solution is approximately given by a simple wave on the C^+, or principal, characteristics (see section 4).

A second feature of interest in figure 2 is that for any given Mach number and deflection angle the jump in r^- is significantly smaller than that in s. At $M_1 = 5$ and $\theta_2 = 0.2$, for example, $\Delta s = 0.19$ while Δr^- is only 0.03. Therefore, for weak to moderate strength shock waves, the flow in the upper half plane can be regarded as primarily an interaction between the simple wave and an entropy variation, with r^- playing only a small role.

With this in mind we introduce a coordinate system (α,β) consisting of the the streamlines, α = constant, and the principal (C^+) characteristics, β = constant. By definition, α and β must satisfy

$$\alpha_x + \alpha_y \tan\theta = 0, \qquad \beta_x + \beta_y \tan(\theta+\mu) = 0. \tag{11}$$

Since any function of α will satisfy the first equation and any function of β will satisfy the second, two conditions will be required later to fix the transformations.

In the new coordinate system (2) becomes

$$s_\beta = 0, \tag{12}$$

or $s = s(\alpha)$. Similarly (3) and (4) become

$$(\theta+P(\mu))_\alpha = \frac{1}{2\delta} \sin 2\mu\, s'(\alpha), \tag{13}$$

$$\left(\frac{\partial}{\partial\alpha} + w \frac{\partial}{\partial\beta}\right)(\theta-P(\mu)) = -\frac{1}{2\delta} \sin 2\mu\, s'(\alpha), \tag{14}$$

where

$$w = \frac{\beta_x + \beta_y \tan(\theta-\mu)}{\alpha_x + \alpha_y \tan(\theta-\mu)} = -\frac{2}{1 - \tan\theta \tan\mu} \frac{x_\alpha}{x_\beta}. \tag{15}$$

The second expression for w follows from (11) and the functional relation

$$\begin{pmatrix} \alpha_x & \alpha_y \\ \beta_x & \beta_y \end{pmatrix} = \frac{1}{x_\alpha y_\beta - y_\alpha x_\beta} \begin{pmatrix} y_\beta & -x_\beta \\ -y_\alpha & x_\alpha \end{pmatrix}. \tag{16}$$

Using (15) and (13), equation (14) can be simplified to

$$(\theta-P(\mu))_\beta = (1 - \tan\theta \tan\mu) \frac{x_\beta}{x_\alpha} \theta_\alpha. \tag{17}$$

Since x and y are now dependent variables, two additional equations are required for them. These are furnished by (11), which by (16) can be written as

$$y_\beta = x_\beta \tan \theta, \qquad y_\alpha = x_\alpha \tan(\theta+\mu). \tag{18}$$

Equations (12), (13), (17), and (18) are five equations in five unknowns: θ, μ, s, x, and y.

It is possible to eliminate y from the equations immediately by setting $y_{\beta\alpha} = y_{\alpha\beta}$ in (18). This gives

$$0 = [\tan\theta - \tan(\theta+\mu)]\frac{x_{\alpha\beta}}{x_\alpha} + \theta_\alpha \sec^2\theta \frac{x_\beta}{x_\alpha} - (\theta+\mu)_\beta \sec^2(\theta+\mu),$$

which, using (17), can be written

$$0 = \frac{x_{\alpha\beta}}{x_\alpha} + (\mu+P(\mu))_\beta \cot\mu + (\theta+\mu)_\beta \tan(\theta+\mu). \tag{19}$$

The first and third terms are the β derivatives of $\log x_\alpha$ and $-\log\cos(\theta+\mu)$, respectively. The second term can also be integrated explicitly; the result is $\lambda \log a$, where we recall $\lambda = (\gamma+1)/(\gamma-1)$. Therefore (19) has as a first integral

$$x_\alpha = A(\alpha)\, a^{-\lambda}\cos(\theta+\mu), \tag{20}$$

where $A(\alpha)$ is an arbitrary function to be determined later. Hence x can be written

$$x(\alpha,\beta) = x(0,\beta) + \int_0^\alpha A(\alpha)\, a^{-\lambda}\cos(\theta+\mu)\, d\alpha. \tag{21}$$

Similarly, from (18) we get

$$y(\alpha,\beta) = y(0,\beta) + \int_0^\alpha \lambda(\alpha) a^{-\lambda} \sin(\theta+\mu)\, d\alpha. \qquad (22)$$

So far α and β have not been specified beyond saying α = constant on streamlines and β = constant on C+ characteristics. The boundary and shock conditions in the $\alpha\beta$-plane can be simplified somewhat by normalizing α and β appropriately. We let the airfoil surface be $\alpha = 0$, and normalize β by setting $\beta = x$ at $\alpha = 0$. The boundary condition (6) then becomes

$$x(0,\beta) = \beta, \quad y(0,\beta) = f(\beta), \quad \theta(0,\beta) = \tan^{-1} f'(\beta). \qquad (23)$$

One convenient way of normalizing α is to take the front shock angle $\eta(\alpha)$ to be given by

$$\tan \eta(\alpha) = (1-\alpha) \tan \eta(0) + \alpha \tan \mu_0, \qquad (24)$$

where $\eta(0)$ is known from solving the shock conditions at the leading edge, and μ_0 is the upstream Mach angle, which the shock approaches far away from the airfoil. (We assume that η is a strictly decreasing function.) The flow field in the upper half plane thus is mapped into a finite region in the $\alpha\beta$-plane, as shown in figures 4 and 9. The principal characteristics become vertical lines, and the streamlines become horizontal lines. The front shock maps into some curve $\beta(\alpha)$, and the rear shock into two separate curves $\beta_2(\alpha)$ and $\beta_3(\alpha)$. Flow variables on $\beta_2(\alpha)$ denote values just to the left of the rear shock, and those on $\beta_3(\alpha)$ denote the

values just to the right. The discussion of these is left to appendix B.

With the shock angle $\eta(\alpha)$ a given function, the shock conditions (7)-(9) can be immediately solved for $\theta(\alpha,\beta(\alpha))$, $\mu(\alpha,\beta(\alpha))$, and $s(\alpha)$. The shock $\beta(\alpha)$ itself will in general depend on the rest of the solution, however.

At $\beta = \beta(\alpha)$ the condition

$$\tan\eta = \frac{dy}{dx} = \frac{y_\alpha + y_\beta \beta'(\alpha)}{x_\alpha + x_\beta \beta'(\alpha)},$$

must be satisfied. Using (18), this can be written

$$x_\alpha + b(\alpha) x_\beta = 0 \quad \text{on} \quad \beta = \beta(\alpha), \tag{26}$$

where

$$b(\alpha) = \beta'(\alpha) \left.\frac{\tan\eta - \tan\theta}{\tan\eta - \tan(\theta+\mu)}\right|_{\beta=\beta(\alpha)}.$$

Substitution of (21) for x in (26) gives a linear integral equation for $A(\alpha)$:

$$A(\alpha) Q(\alpha,\beta(\alpha)) + b(\alpha)\left[1 + \int_0^\alpha A(\sigma) Q_\beta(\sigma,\beta(\alpha))\, d\sigma\right] = 0 \tag{27}$$

where $Q = a - \lambda\cos(\theta+\mu)$. If the solution for θ, μ, and s is known in the $\alpha\beta$-plane, this equation can be solved for $A(\alpha)$, and the transformation back to the physical plane computed with (21) and (22). In general however the solution in the $\alpha\beta$-plane depends on x through (17).

Up to this point the equations in $\alpha\beta$-coordinates have

been derived without approximation, and hence are equivalent to the original set (2)-(4).

4. Approximate solutions

Simple wave approximation

As mentioned earlier, in a problem with weak shock waves deviations in s and r⁻ from their upstream values are third-order quantities and can be neglected; that is, it can be assumed that $s = 0$ and $r^- = -P(\mu_0)$ everywhere. The solution of (2)-(4) then is a simple wave, in which all quantities are constant on the principal characteristics, which in turn are straight lines:

$$\theta = \tan^{-1} f'(\beta), \quad \mu = P^{-1}(\theta + P(\mu_0)), \quad s = 0$$

$$\text{on} \quad C^+: \; y = f(\beta) + (x-\beta)\tan(\theta+\mu).$$

This approximation is due to Friedrichs (1948). (Friedrichs further simplified the problem by neglecting terms of third order and higher throughout the calculation.) The solution satisfies the boundary condition, but can satisfy only one of the three conditions at the shock. However, since two quantities (s and r^-) are conserved up to third order across the shock, if one condition is satisfied the other two will be satisfied up to third order. It is convenient to retain the shock condition on θ, equation (7), which can be solved

for the shock angle η as a function of $\theta(\beta)$. Denoting the shock by $[X(\beta), Y(\beta)]$ we have then

$$Y(\beta) = f(\beta) + [X(\beta) - \beta]\tan(\theta+\mu),$$
$$Y'(\beta)/X'(\beta) = \tan\eta.$$

Eliminating $Y(\beta)$ between these two produces a linear first-order ordinary differential equation for $X(\beta)$, for which an explicit solution is easily found.

Shock expansion theory

Because simple wave theory takes s and r^- constant at their upstream values, it can be expected to be least accurate near the airfoil, where the shock is strongest and the deviation from upstream conditions is the greatest. An improved approximation in this region can be obtained using shock expansion theory, in which s and r^- are assumed to be everywhere equal to their values behind the shock at the leading edge, say $s = s_0$ and $r^- = \bar{r_0}$. This leads to a slightly modified version of the simple wave solution, namely

$$\theta = \tan^{-1} f'(\beta), \quad \mu = P^{-1}(\theta - \bar{r_0}), \quad s = s_0$$
$$\text{on } C^+: \; y = f(\beta) + (x-\beta)\tan(\theta+\mu).$$

This approximation produces a very accurate solution at the airfoil, even for flows with strong shocks, in which s and r^- are not at all constant globally. Errors should be

expected because the C- (compression) waves which are produced by reflection of the C+ (expansion) waves at the front shock have been neglected. Hayes & Probstein (1966) explain that these reflections however are fairly weak, and, more importantly, are nearly cancelled by expansion waves produced by the interaction of the C+ waves with the entropy or vorticity layers. Mahony (1955) gives a similar explanation.

The shock expansion solution rapidly loses accuracy as the distance from the airfoil increases. This is in contrast to simple wave theory, which is accurate at infinity.

Present approximation

We make the assumption that the flow angle θ is approximately constant on principal characteristics. This holds true in the simple wave solution, and in general is closely related to shock expansion theory. This relationship will be brought out later. If $\theta_\alpha = 0$, then (17) reduces to

$$(\theta - P(\mu))_\beta = 0 \quad \text{or} \quad \theta - P(\mu) = -P_0(\alpha), \tag{28}$$

where $P_0(\alpha) = P[\mu(\alpha, \beta(\alpha))] - \theta(\alpha, \beta(\alpha))$ is given explicitly by the shock conditions. Substitution of $\theta = P(\mu) - P_0(\alpha)$ in the remaining equation, (13), then gives

$$2P(\mu)_\alpha - P_0'(\alpha) = \frac{1}{2\pi} \sin 2\mu \; s'(\alpha). \qquad (29)$$

$P_0(\alpha)$ and $s(\alpha)$ are known functions, so (29) can be regarded as an ordinary differential equation for μ, in which β enters only as a parameter, through the initial value

$$\mu(0,\beta) = P^{-1}[P_0(0) + \tan^{-1} f'(\beta)].$$

Equation (29) is nonlinear, but can be readily solved using standard numerical methods. The solution in the $\alpha\beta$-plane is then completed by computing $\theta(\alpha,\beta) = P(\mu(\alpha,\beta)) - P_0(\alpha)$ and finding the shock $\beta(\alpha)$ from the computed solution $\mu(\alpha,\beta)$ and the values $\mu(\alpha,\beta(\alpha))$ given by the shock conditions. (Since in practice this would involve interpolation, it is more convenient to use $\mu(\alpha,\beta(\alpha))$ as the initial value and integrate (29) downwards along each characteristic $\beta = \beta(\alpha)$. Then $\beta(\alpha)$ can be computed from

$$f'(\beta(\alpha)) = \tan\{P[\mu(0,\beta(\alpha))] - P_0(0)\}$$

by inverting f'.) The solution for θ, μ, and s in the $\alpha\beta$-plane is independent of x and y, because (17), the only equation in which x or y appears, is neglected. The transformation back to the xy-plane is found by solving (27) for $\Lambda(\alpha)$ (also an easy numerical calculation) and evaluating the integrals (21) and (22). The solution obtained from this approximation will satisfy the boundary condition and all three shock conditions, but will satisfy (17) only approximately.

This approximation is related to shock expansion theory in the following way. Shock expansion theory shows that r^- is approximately constant along the airfoil, and, as has been pointed out by Mahony and Skeat (1955) and Meyer (1957), since any streamline is a potential airfoil, r^- should be approximately constant along each streamline. This is just (28).

In the literature this assumption is employed in various ways. If $r^- = -P_0(\alpha)$, then by (17) $\epsilon = \epsilon(\beta)$, and hence also $p = p(\beta)$, as can be seen from (5+). Taking both $\epsilon = \epsilon(\beta)$ and $p = p(\beta)$ along with $r^- = -P_0(\alpha)$ overdetermines the problem however, since any one of θ, p, and r^- can be written as a function of the other two (and s). This was noted by Eggers, Syvertson, and Kraus (1953). In their generalized shock expansion method (a numerical construction similar to the method of characteristics), they resolve this by averaging results assuming $r^- = -P_0(\alpha)$ and $\theta = \theta(\beta)$ with those assuming $r^- = -P_0(\alpha)$ and $p = p(\beta)$. While this seems somewhat arbitrary, it can be shown that the correct result in fact lies between the two (see Hayes & Probstein 1966, p. 498). Meyer (1957), on the other hand, implicitly drops the assumption $p = p(\beta)$, and uses the solution $r^- = -P_0(\alpha)$ and $\epsilon = \epsilon(\beta)$, which satisfies (17) exactly, but does not satisfy (13).

It is more consistent to approach the problem in either of two ways: in equation (17) assume (i) the left hand side or (ii) the right hand side is zero. Then solve (17) along

with the remaining equation, (13). In case (i), the solution becomes $\theta = \theta(\beta)$, $p = p(\beta)$, and $s = s(\alpha)$. The function $\theta(\beta)$ is determined by the boundary condition, and $p(\beta)$ must be determined by the shock conditions. It then happens that over the rear half of the airfoil, $\beta > \beta(1)$, $p(\beta)$ cannot be found, since no data is specified on the rear shock. This difficulty does not arise in approach (ii), which is the one we adopt. This method requires more work, but has been found to be more accurate. It also produces the same solution at the airfoil as shock expansion theory. Additional support for this choice is lent by the fact that the factor multiplying e_α in (17) is in general quite small. Approach (i) has however been found useful for calculating the flow behind the tail shock, where the other method is inappropriate (see appendix B).

5. Numerical method

Our approximate solution does not satisfy (17), or, equivalently, the C^- equation (14). In this section we present a simple iterative method for correcting the solution so that it will satisfy all the equations and conditions.

The approximate solution is first computed on a rectangular grid in the $\alpha\beta$-plane, as shown in figures 4 and 9. The same grid points are used in the iteration scheme.

The front shock $\beta(\alpha)$ is therefore kept fixed throughout the iterations. This fixes the normalization of α, so for every iteration beyond the original approximation $\eta(\alpha)$ is not given by (24) and must be found as part of the solution. This also implies that $\alpha=1$ will no longer correspond exactly to $y=\infty$.

Given the approximate solution for θ, μ, s, and x in the $\alpha\beta$-plane, a corrected value of r^- is computed from the C^- equation, (14), starting at the shock with the value given by the shock conditions and integrating along C^- characteristics:

$$r^- = r^-_{shock} - \int_{C^-} \frac{1}{2\theta} \sin 2\mu \, ds. \tag{30}$$

The new value $r^-(0,\beta)$ at the airfoil determines a new value of r^+ there, since $r^+ = 2\theta - r^-$, and $\theta(0,\beta)$ is given by the boundary condition. With this as an initial value, a new r^+ can be computed everywhere by integrating (13) along C^+ characteristics:

$$r^+(\alpha,\beta) = r^+(0,\beta) + \int_0^\alpha \frac{1}{2\theta} \sin 2\mu \, s'(\alpha) \, d\alpha. \tag{31}$$

The solution given by r^-, r^+, and s will satisfy (13), (14), and the boundary condition. However, the new value of $r^+(\alpha,\beta(\alpha))$ will not in general satisfy the shock conditions, and hence will imply new values of $\eta(\alpha)$, $s(\alpha)$, and $r^-(\alpha,\beta(\alpha))$. This furnishes a new initial value for integrating (30), which is used to start the next iteration.

In summary, the steps of the method are as follows:

I. Compute approximation, fixing front shock and grid in $\alpha\beta$-plane.

II. Compute $r^-(\alpha,\beta(\alpha))$ from the shock conditions and $r^-(\alpha,\beta)$ everywhere from (30).

III. Compute new $r^+(0,\beta) = 2\theta(0,\beta) - r^-(0,\beta)$ with $\theta(0,\beta)$ from the boundary condition and $r^-(0,\beta)$ from step II. Compute $r^+(\alpha,\beta)$ everywhere from (31).

IV. Compute new values $\theta = (r^+ + r^-)/2$ and $\mu = p^{-1}((r^+ - r^-)/2)$ everywhere. With the new solution at the shock compute a new $\eta(\alpha)$ and $s(\alpha)$ from the shock conditions. Also recompute $A(\alpha)$ and $x(\alpha,\beta)$.

V. Check for convergence and either go to step II or stop and compute $y(\alpha,\beta)$.

This scheme has been implemented using second-order numerical methods (trapezoidal rule, etc.). The details are given in appendix C.

The evaluation of the integral (30) at step II is the most complicated calculation in the procedure. In place of equation (14) we might have integrated (17), which is equivalent and has the advantage that r^- is differentiated only with respect to β. In practice however, this does not work very well. The iteration procedure does not converge as quickly, and may not converge at all without modification (see Chong & Sirovich 1980). We attribute this to the fact that small variations in r^- are naturally propagated along the C^- characteristics.

6. Results and discussion

The execution of the numerical procedures which we have discussed is both rapid and inexpensive. As a result we have performed a number of calculations for several airfoils over a range of Mach numbers. The results presented in the figures are for a symmetric circular arc airfoil with thickness ratio 0.25, at upstream Mach numbers M_0 = 2.5 and 7.5. In some figures the intermediate case M_0 = 4.0 is also shown. These cases were chosen in part for the interesting effects they exhibit.

The iteration scheme is found to converge quite rapidly, based on a comparison of the solutions at succesive iterations. In the following table, the maxima (over all grid points) or the differences in the values of θ, μ, and x are given for the case M_0=7.5.

iteration	$\Delta\theta/\theta(J,0)$	$\Delta\mu/\mu$	$\Delta x/x$
1	0.0595	0.1170	0.3701
2	0.0141	0.0096	0.1221
3	0.0008	0.0007	0.0112
4	0.0002	0.0006	0.0017
5	0.0001	0.0003	0.0009

The greatest differences are in x and occur within a few grid points of α=1, where $x \to \infty$. The errors in x are smaller closer to the airfoil. For thinner airfoils and/or lower

Mach numbers, fewer iterations are required for the same accuracy. In the case of a 10% thick parabolic arc airfoil, for example, even at $M_0=10$ the difference between the approximate and exact solutions is less than one percent in θ and p and six per cent in x. In such a case there is little reason to go beyond the approximate solution.

The case $M_0=2.5$ is discussed in Holt (1977). Figure 3 contains a comparison of the leading shock when computed by our method and the BVLR method. The small difference is probably attributable to copying errors. In addition we indicate our approximate theory and that which emerges from a variant of shock expansion theory (the latter and the BVLR curve are taken from Holt, p.77). In this case, our approximate solution is indistinguishable from the exact solution.

We continue the presentation of this case by indicating in figure 4 a portion of the grid in the $\alpha\beta$-plane used in the numerical integration. (The increment $\Delta\alpha$ between the streamlines shown is 0.1; the computations were done with $\Delta\alpha=0.025$.) The triangular region corresponds to the flow behind the tail shock (see appendix B). Figure 5 gives the entropy $s(\alpha)$ in the region between the front and tail shocks, and $s_3(\alpha)$ in the region behind the tail shock. The deflection angle θ is plotted versus α in figure 6 on each of the C^+ characteristics shown in figure 4. A specification of θ in the region behind the tail shock is deemed unnecessary since it is very nearly zero everywhere

($|\theta|<0.005$). Figure 7 contains the variation of r^- versus on each streamline of figure 4. Finally, in figure 8 the streamlines, characteristics, and shock waves are shown transformed back to the xy-plane. These figures completely determine the solution. In particular, corresponding to any point (x,y) of the physical plane we can determine the coordinates (α,β). The entropy s is then found from figure 5 and the deflection angle θ from figure 6. The latter and r^- from figure 7 determine the Prandtl angle $P(\mu)$. All other flow properties then follow.

For comparison we give in figures 9-13 similar data for the same profile at $M_0=7.5$. In this case $|\theta|<0.02$ behind the tail shock.

We begin our discussion of these results by considering the limit $x \to \infty$. Far behind the airfoil the pressure becomes constant, $p \to 1$, and as a consequence $\theta \to 0$. It then follows from the equation of state that

$$a^2 = \exp[-(\gamma-1)s_3(\alpha)/\gamma],$$

where $s_3(\alpha)$ is given either by figure 5 or figure 10. From (1), we can then compute the velocity q at infinity. This is shown in figure 14 for $M_0 = 2.5$, 7.5, and the intermediate case $M_0 = 4.0$ (same profile). As a result of the non-uniform entropy, the flow at infinity has a vorticity distribution.

Another feature of interest is the entropy variation along the tail shock (figures 5 and 10). This has a

two-scale appearance, especially at the higher Mach number, which shows a very rapid decrease in strength in the initial portion of the shock. The slower variation in entropy follows that induced by the front shock. Looking at figure 13, we see that the streamlines spread apart rapidly as the flow passes the midchord position. The flow inclination at the tail shock therefore decreases rapidly, which results in a corresponding decrease in shock strength.

Another important effect is also at work in this region. The gas, which is compressed at the front shock, in following the profile past the midchord experiences a rapid expansion, which is sufficiently strong so that the local Mach number at the trailing edge exceeds the upstream value ($M = 9.33$ for the $M_o = 7.5$ case). Since μ is small, the large negative value of θ on the after part of the airfoil causes the principal characteristics to have negative slopes, so that waves originating there must intersect the tail shock near the airfoil. This quickly cuts off the recovery process. As a result the Mach number along the tail shock falls off rapidly, which augments the rapid decrease in strength of the tail shock. For the case $M_o = 7.5$ the Mach number along the shock even falls below 7.5.

A feature which is somewhat difficult to perceive from figures 8 and 13 is that the tail shock angle is not monotonic. In figure 15 the variation of the slope of the tail shock is given for the three cases we have discussed.

For each case the shock angle decreases on leaving the trailing edge. (This result has been verified independently by James C. Townsend 1979, using a different numerical method developed by Manuel D. Salas.) This is contrary to what is observed for lower Mach numbers or thinner bodies. We have seen that the angle of the incident flow decreases along the shock. If the Mach number to the left of the shock were constant, this would predict a decrease in shock angle. The decrease in Mach number along the shock tends to have the opposite effect however, to increase the shock angle. In these cases, near the trailing edge the decreasing flow angle dominates. For high Mach numbers the shock angle is more dependent on the flow angle than on the Mach number, as can be seen from the fact that the shock polars for different Mach numbers approach a limiting curve as $M \to \infty$ (see e.g. Liepmann & Roshko 1957, p. 87). For lower Mach numbers or thinner airfoils the effect of decreasing Mach number dominates the effect of decreasing flow angle.

Returning to figure 15 we also see that for $M_0 = 7.5$ the slope undergoes a second oscillation in which it rises above the Mach angle at infinity. This is explained by the rapid fall-off of Mach number along the shock, below its value at infinity. A final item of note in figure 15 is that for $M_0 = 7.5$ the shock slope actually starts off with a value which is greater than at infinity. The expansion process along the profile produces a relatively high Mach number at

the trailing edge, but it is not great enough to bring the slope below the upstream value.

The pressure distribution behind the airfoil is interesting. In figures 16 and 17 we show the pressure contours behind the tail shock and the values of log p on the x-axis for x>1, for the cases M_0 = 2.5 and 7.5. The pressure on the rear part of the airfoil is so low that, in spite of the high shock strength at the trailing edge, the pressure jump through the shock does not bring p up to the equilibrium pressure p=1. There is a rapid pressure increase immediately behind the trailing edge, in which p increases above the equilibrium value, reaching a maximum about one chord length out. The return to equilibrium from this point is very gradual. The total variation in pressure behind the tail shocks is quite small compared to that along the airfoil surface (in terms of log p, about 3% at M_0=2.5 and 10% at M_0=7.5).

Several other features of the calculations also merit mention. Most notable perhaps is the surprising constancy of the deflection angle on the principal characteristics. The variation in θ is almost undetectable in figure 6 and, as figure 11 indicates, the most serious departure occurs near the trailing edge, where it is about 10% in the worst case. As mentioned already, ϵ = 0 is an excellent approximation throughout the region behind the tail shock. A related phenomenon is the near-straightness of the principal characteristics. This however does not remain

true in the region behind the airfoil.

We are also in a position to examine the basic assumption of shock expansion theory, that r^- is constant on streamlines. From equation (17) we see that this condition is closely related to the constancy of θ on principal characteristics. As both figures 7 and 12 indicate, this is a reasonable assumption, although somewhat remarkably it is better at the airfoil than in its neighborhood. In both cases this assumption is far less satisfactory behind the tail shock. The rapid down stroke of the r^- curves also indicates a large value of θ_α, although θ itself remains quite small.

This work was supported by the National Aeronautics and Space Administration under NASA Grant no. NSG 1617.

Appendix A: Case of an arbitrary gas

For an arbitrary gas, the equations of motion in characteristic form can be written (Hayes & Probstein 1966, p. 484)

$$ds = 0 \quad \text{on} \quad dy/dx = \tan\theta \tag{A1}$$

$$d\theta \pm \Phi\, dp = 0 \quad \text{on} \quad dy/dx = \tan(\theta \pm \mu) \tag{A2}$$

where $\Phi = p_o/(\rho_o a_o^2 \rho q^2 \tan\mu)$. We can consider Φ to be a

function of p and s. By introducing the variables

$$\omega(p,s) = \int \Phi(p,s)\,dp \quad \text{and} \quad \Omega(p,s) = \partial\omega(p,s)/\partial s,$$

which are defined so that $d\omega = \Phi\,dp + \Omega\,ds$, (A2) can be written

$$d\theta \pm d\omega = \pm \Omega\,ds \quad \text{on} \quad dy/dx = \tan(\theta\pm\mu) \tag{A3}$$

If ω and Ω are now regarded as functions of μ and s, (A1) and (A3) are three equations in three unknowns: θ, μ, and s. Equations (3) and (4) are a special case of (A3) in which $\omega = P(\mu)$ and $\Omega = (\sin 2\mu)/2\mu$.

The transformation to $\alpha\beta$-coordinates goes through for the most part as before. Equations (12)-(14) in the general case become

$$s_\beta = 0$$

$$(\theta+\omega)_\alpha = \Omega s'(\alpha)$$

$$\left(\frac{\partial}{\partial\alpha} + w\,\frac{\partial}{\partial\beta}\right)(\theta-\omega) = -\Omega s'(\alpha)$$

where w is still given by (15). The counterpart of (19) is

$$0 = \frac{x_{\alpha\beta}}{x_\alpha} + (\mu+\omega)_\beta \cot\mu + (\theta+\mu)_\beta \tan(\theta+\mu)$$

This equation can in principle be solved in the same manner as (19), but we do not have an explicit integral of the simple form (20).

The assumption $\theta_\alpha = 0$ in the general case implies

$(\epsilon - \omega)_\beta = 0$ or $\epsilon - \omega = -\omega_0(\alpha)$. The resulting approximation can be expected to be valid at least in cases in which the behavior of the gas does not differ too greatly from that of a perfect gas with constant specific heats and $\gamma = 1.4$. It has been shown (see Hayes & Probstein 1966, §7.2) that shock expansion theory tends to lose accuracy if γ is allowed to approach 1.

Appendix B: Tail shock for a symmetric airfoil

In the general case, the solutions in the upper and lower half planes can be computed independently, up to the appearance of the tail shocks. The flows from the top and bottom interact behind the airfoil, which complicates the computation of the tail shocks and the flow behind them. The upper and lower regions behind the airfoil are separated by a contact discontinuity, or slipstream, whose location is unknown a priori. Across the slipstream ϵ and p are continuous, but the other variables jump. This complication does not arise in the case of an airfoil symmetric with respect to the x-axis; the slipstream coincides with the x-axis, and can be considered a rigid boundary. The problem is still quite different than the front shock problem, because the flow upstream of the tail shock is not uniform.

The transformation to $\alpha\beta$-coordinates behind the tail shock can be chosen differently than that ahead of it. In

particular, it is more proper to regard the C^- characteristics as the principal characteristics, since the C^+ waves are only produced as reflections of the C^- waves, which originate at the tail shock (see figure 1). On the other hand, we have found that for the iteration procedure it is better to take the C^+ characteristics as the β-coordinates, because this has the effect of putting more points near the trailing edge, where the most rapid variation in the solution occurs. However, the approximate solution derived below is more accurate if the C^- characteristics are taken as β = constant. Modifications for the use of the C^- characteristics as coordinates in place of the C^+ characteristics are straightforward.

The normalizations of α and β behind the tail shock are also different than those ahead of it. It is natural to keep α constant on streamlines as they cross the shock. Also, rather than set $\beta = x(0,\beta)$, we can normalize β so that the region $x>1$ is mapped into a finite region in the $\alpha\beta$-plane. This was done by setting $\beta_3(\alpha) = 1 + \alpha/2$, producing the configurations shown in figures 4 and 9.

The calculation of the tail shock $\beta_2(\alpha)$ can be done as follows. We assume that the solutions for $\theta(\alpha,\beta)$, $\mu(\alpha,\beta)$, and $x(\alpha,\beta)$ are known in the neighborhood of $\beta_2(\alpha)$. Equation (26) holds at $\beta_2(\alpha)$ as well as at $\beta(\alpha)$, and since in the former case x_α and x_β are known functions, we can write (26) as an ordinary differential equation for $\beta_2(\alpha)$:

$$\beta_2'(\alpha) = B(\alpha, \beta_2(\alpha)) = -\frac{\tan\eta_2 - \tan(\theta+\mu)}{\tan\eta_2 - \tan\theta}\,\frac{x_\alpha}{x_\beta}\qquad \beta=\beta_2(\alpha) \tag{B1}$$

As yet $\eta_2(\alpha)$ is undetermined. If we specify one variable, say θ, just to the right of the shock [i.e. at $\beta = \beta_3(\alpha)$] then we can solve the shock conditions for $\eta_2(\alpha)$, and solve (B1). This enables us to set up an iteration procedure similar to that used for the front flow.

The approximate solution used for the flow over the airfoil cannot be conveniently employed for the flow behind the tail shock, because the nonuniform flow to its left makes it impossible to calculate $P_0(\alpha)$ and $s(\alpha)$ a priori for use in (29). Therefore we use the simpler of the approximations given in section 4: $\theta = \theta_3(\beta)$, $p = p_3(\beta)$, and $s = s_3(\alpha)$. All the characteristics intersect the x-axis, where $\theta = 0$, so $\theta_3(\beta) = 0$, and hence $\theta = 0$ everywhere. In particular $\theta = 0$ at $\beta = \beta_3(\alpha)$. We can therefore solve for $\beta_2(\alpha)$ as in the previous paragraph, and also compute all other quantities on both sides of the shock. This determines $p_3(\beta)$ and $s_3(\beta)$.

The computation of the transformation from $\alpha\beta$- to xy-coordinates is also somewhat different. Denoting the known value $x(\alpha, \beta_2(\alpha))$ by $x_2(\alpha)$, we must have $x(\alpha, \beta_3(\alpha)) = x_2(\alpha)$, which implies

$$x_2'(\alpha) = x_\alpha(\alpha, \beta_3(\alpha)) + \beta_3'(\alpha)\, x_\beta(\alpha, \beta_3(\alpha)). \tag{B2}$$

An equation of the form (26) also holds at $\beta = \beta_3(\alpha)$:

$$\vartheta = x_\alpha(\alpha, \beta_3(\alpha)) + b_3(\alpha)\, x_\beta(\alpha, \beta_3(\alpha)). \tag{B3}$$

If we eliminate x_β between these two, substitute $x_\alpha = A_3(\alpha) Q(\alpha, \beta)$ [where we recall $Q = a - \lambda \cos(\theta+\mu)$], and solve for $A_3(\alpha)$, we get

$$A_3(\alpha) = \frac{x_2'(\alpha)}{Q(\alpha, \beta_3(\alpha))} \left. \frac{\tan \eta_2(\alpha) - \tan \theta}{\tan(\theta+\mu) - \tan \theta} \right|_{\beta = \beta_3(\alpha)} \tag{B4}$$

from which we can determine

$$x(\alpha, \beta) = x_2(\alpha_3(\beta)) + \int_{\alpha_3(\beta)}^{\alpha} A_3(\sigma)\, Q(\sigma, \beta)\, d\sigma \tag{B5}$$

where $\alpha_3(\beta)$ denotes the inverse of $\beta_3(\alpha)$. A similar equation follows for $y(\alpha, \beta)$.

The iteration scheme proceeds essentially as before. Given $r^-(\alpha, \beta_3(\alpha))$ from the shock conditions, we integrate (30) along C^- characteristics down to the slipstream $\alpha = 0$. Then we reset $r^+(0, \beta) = -r^-(0, \beta)$, and integrate (31) upwards to $\beta_3(\alpha)$. The new r^+ and r^- define a new $\theta(\alpha, \beta_3(\alpha))$, which is used to solve for a new shock $\beta_2(\alpha)$ and new functions $\eta_2(\alpha)$, $s_3(\alpha)$, and $r^-(\alpha, \beta_3(\alpha))$, with which we start the next iteration.

Appendix C: Details of numerical method

This appendix contains the details of each step of the iteration scheme described in section 5, as presently

implemented.

Step I. We take a uniform grid in α with N+1 points $\alpha_i = i\Delta\alpha$ (i=0,1,...,N), where $\Delta\alpha = 1/N$. Over the front half of the airfoil the β grid points are taken to be $\beta_j = \beta(\alpha_j)$ (j=0,1,...,N), where $\beta(\alpha)$ is the equation of the shock as given by the approximate solution. Over the rear half of the airfoil the β grid points are taken evenly spaced.

The approximate solution in the $\alpha\beta$-plane requires the solution of the ordinary differential equation (29) for each β_j. This was done by the improved Euler method, which for the general equation $d\xi/dt = \varphi(\xi,t)$ is given by

$$\xi_{k+1} = \xi_k + \frac{\Delta t}{2}[\varphi(t_k,\xi_k) + \varphi(t_{k+1},\xi_k+\Delta t\,\varphi(t_k,\xi_k))] \qquad (C1)$$

The approximate solution is completed by solving the integral equation (27) for $A(\alpha)$ and evaluating x and y from (21) and (22). Equation (27) is linear, and can be readily solved by the trapezoidal rule: the integral is approximated by the appropriate sum, and the resulting equation is solved for $A(\alpha_j)$ in terms of $A(\alpha_0)$, $A(\alpha_1)$,..., $A(\alpha_{j-1})$. The derivatives $Q_\beta(\alpha_i,\beta_j)$ appearing in the integral are evaluated numerically using a three point scheme on the uneven β mesh. The integrals for x and y, (21) and (22), are computed by the trapezoidal rule.

Step II. We can write (14) as

$$dr^- = -\frac{1}{2\pi}\sin 2\mu\, ds \quad \text{on} \quad C^-: \; d\beta/d\alpha = w \qquad (C2)$$

where w is given by (15). In computing w, x_β must be evaluated numerically, but x_α is given analytically by (20). The C⁻ characteristic through the point (α,β) is drawn back to intersect the line segment between $(\alpha,\beta-\Delta\beta)$ and $(\alpha+\Delta\alpha,\beta)$ at the point $(\hat{\alpha},\hat{\beta}) = (\alpha+\nu\Delta\alpha,\beta+(\nu-1)\Delta\beta)$. To find this point the equation $d\beta/d\alpha = w$ is integrated from α to $\hat{\alpha}$, using the improved Euler method (C1) again, with the modification that a first approximation to $w(\hat{\alpha},\hat{\beta})$ must be found by interpolation. We take

$$\nu = \left[1 - w(\alpha,\beta)\frac{\Delta\alpha}{\Delta\beta}\right]^{-1}$$

$$\hat{w} = (1-\nu)\,w(\alpha,\beta-\Delta\beta) + \nu\, w(\alpha+\Delta\alpha,\beta)$$

and then redefine ν by

$$\nu = \left[1 - \tfrac{1}{2}(w(\alpha,\beta)+\hat{w})\frac{\Delta\alpha}{\Delta\beta}\right]^{-1}$$

This value is correct to second order and is used to interpolate the value

$$\hat{r}^- = (1-\nu)\,r^-(\alpha,\beta-\Delta\beta) + \nu\, r^-(\alpha+\Delta\alpha,\beta)$$

and, similarly, μ and $\hat{s}$. The value of $r^-(\alpha,\beta)$ is then computed by the trapezoidal rule:

$$r^-(\alpha,\beta) = \hat{r}^- - \frac{1}{4\nu}[\sin 2\mu(\alpha,\beta) + \sin 2\hat{\mu}][s(\alpha)-\hat{s}].$$

A somewhat simpler method can be used if (α,β) is two or more grid points from the shock. We write (14) as

$$r^-_\alpha + w r^-_\beta = - \frac{1}{2\rho} \sin 2\mu \, s'(\alpha),$$

evaluating w and μ at (α,β), and replacing r^-_α and r^-_β by three-point one-sided differences employing points upward and to the left of (α,β), respectively. Then we solve for $r^-(\alpha,\beta)$.

Step III. Equation (13) can be integrated directly. Again using the trapezoidal rule, we have

$$r^+(\alpha+\Delta\alpha,\beta) = r^+(\alpha,\beta) + \frac{1}{4\rho}[\sin 2\mu(\alpha,\beta) + \sin 2\mu(\alpha+\Delta\alpha,\beta)][s(\alpha+\Delta\alpha) - s(\alpha)]. \tag{C3}$$

Step IV. While it is possible in theory to solve the shock relations given any one quantity just to the right of the shock, in practice it is difficult given r^+ or r^-. Therefore we use the new $\theta(\alpha,\beta)$ computed from r^+ and r^-, and solve the shock relations for $\eta(\alpha)$, $s(\alpha)$, and $\mu(\alpha,\beta(\alpha))$ as functions of $\theta(\alpha,\beta(\alpha))$. Then $r^-(\alpha,\beta(\alpha))$ is redefined from these values to start step II.

The computations of $A(\alpha)$ and $x(\alpha,\beta)$ are done in the same way as in the approximate solution. It is not necessary to compute $y(\alpha,\beta)$ until the final solution is obtained, since only x appears in the equations.

Step V. To check for convergence, we compare θ, μ, and x at all grid points between successive iterations, and stop when the maximum difference is less than some given tolerance.

References

Adamson, T. C. 1968 J. Fluid Mech. 34, 735.

Babenko, K. I., Voskresenskiy, G. P., Lyubimov, A. N. & Rusanov, V. V. 1966 Three-dimensional flow of ideal gas past smooth bodies. NASA Tech. Transl. F-380.

Chong, T. H. & Sirovich, L. 1980 To appear in Phys. Fluids.

Courant, R. & Friedrichs, K. O. 1948 Supersonic Flow and Shock Waves. Interscience.

Eggers, A. J., Syvertson, C. A. & Kraus, S. 1953 NACA Report no. 1123.

Epstein, P. S. 1931 Proc. Nat. Acad. Sci. 17, 532.

Friedrichs, K. O. 1948 Comm. Pure Appl. Math. 1, 211.

Hayes, W. D. & Probstein, R. F. 1966 Hypersonic Flow Theory, vol. I. Academic Press.

Holt, M. 1977 Numerical Methods in Fluid Dynamics. Springer-Verlag.

Liepmann, H. W. & Roshko, 1957 Elements of Gasdynamics. Wiley.

Lighthill, M. J. 1960 Higher Approximations in Aerodynamic Theory. Princeton University Press.

Jones, J. G. 1963 J. Fluid Mech. 17, 506.

Mahony, J. J. 1955 J. Aero. Sci. 22, 673.

Mahony, J. J. & Skeat P. R. 1955 Austr. Aero. Res. Lab., Aero. Note 147.

Meyer, R. E. 1957 Q. Appl. Math. 14, 433.

Meyer, R. E. 1960 Theory of characteristics in inviscid gas

dynamics, Handbuch der Physik, vol. IX. Springer-Verlag.

Sirovich, L. & Chong, T. H. 1980 To appear in Phys. Fluids.

Taylor, T. D., Ndefo, F. & Masson, B. S. 1972 J. Comp. Phys. 9, 99.

Townsend, J. C. 1979 Private communication.

Figure captions

Figure 1. Supersonic flow past an airfoil: heavy lines denote shock waves; solid lines denote streamlines and C^+ characteristics; dashed lines denote C^- characteristics.

Figure 2. Jumps in entropy s and Riemann invariant r^- across a shock wave as a function of θ_2 ($\theta_1 = 0$) at various Mach numbers. ——, Δs; ----, Δr^-.

Figure 3. Front shock for flow past a 25% circular arc profile at M_o=2.5. -----, BVLR method; —·—, shock expansion method (both from Holt, 1977); ———, present approximate and exact methods.

Figure 4. M_o=2.5. Flow field in $\alpha\beta$-plane.

Figure 5. M_o=2.5. Entropy $s(\alpha)$ (——) in region between front and tail shocks, and $s_3(\alpha)$ (----) in region behind tail shock.

Figure 6. M_o=2.5. Flow angle θ vs. α on each C^+ characteristic of figure 4.

Figure 7. M_o=2.5. Riemann invariant r^- vs. β on each streamline of figure 4.

Figure 8. M_o=2.5. Flow field in xy-plane. The streamlines and C^+ characteristics correspond to the lines α = constant and β = constant, respectively, in figure 4.

Figure 9. M_o=7.5. Flow field in $\alpha\beta$-plane.

Figure 10. M_o=7.5. Entropy $s(\alpha)$ (——) in region between front and tail shocks, and $s_3(\alpha)$ (----) in region behind

tail shock.

Figure 11. M_o=7.5. Flow angle θ vs. α on each C^+ characteristic of figure 9.

Figure 12. M_o=7.5. Riemann invariant r^- vs. β on each streamline of figure 9.

Figure 13. M =7.5. Flow field in xy-plane. The streamlines and C^+ characteristics correspond to the lines α = constant and β = constant, respectively, in figure 9.

Figure 14. Velocity profiles far behind airfoil for M_o = 2.5, 4.0, and 7.5. Dashed lines denote asymptotic values M_o.

Figure 15. Tail shock slope tan η_z vs. α for M_o = 2.5, 4.0, and 7.5. Dashed lines are asymptotic values, tan μ_o.

Figure 16. M_o=2.5. Upper: pressure contours behind tail shock; log p = -0.07(0.01)0 and 0(0.001)0.01. Lower: log p vs. x on x-axis.

Figure 17. M_o=7.5. Upper: pressure contours behind tail shock; log p = -0.5(0.1)0.1 and 0.1(0.02)0.28. Lower: log p vs. x on x-axis.

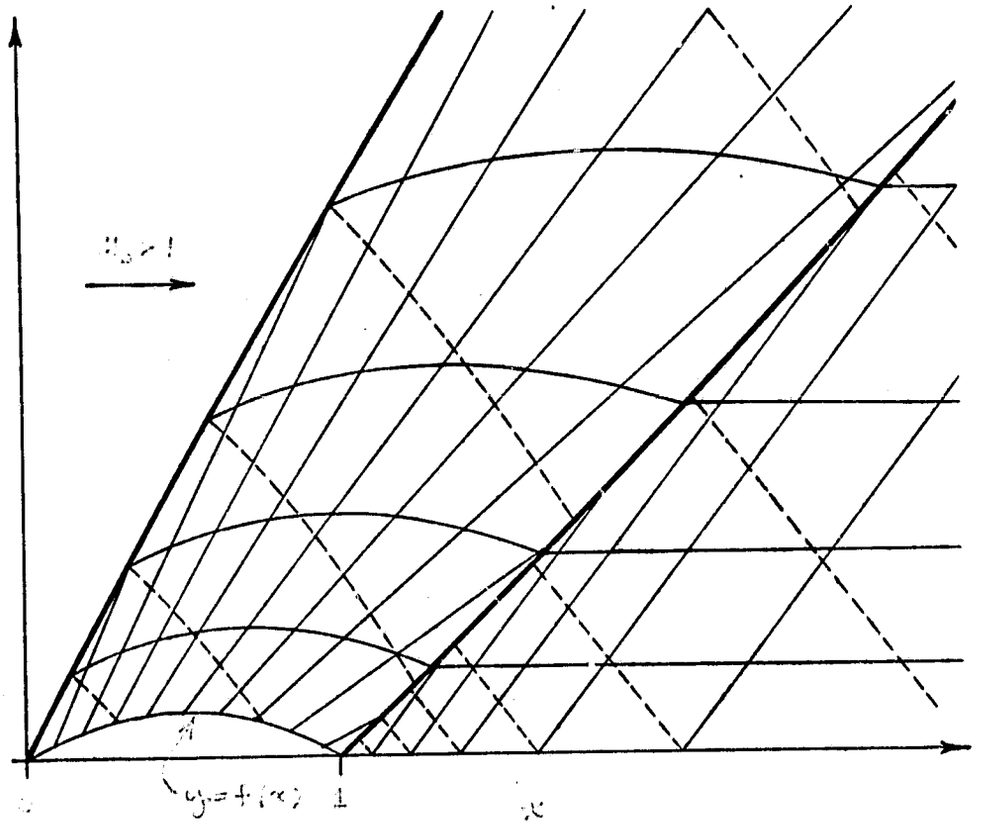

Fig. 1

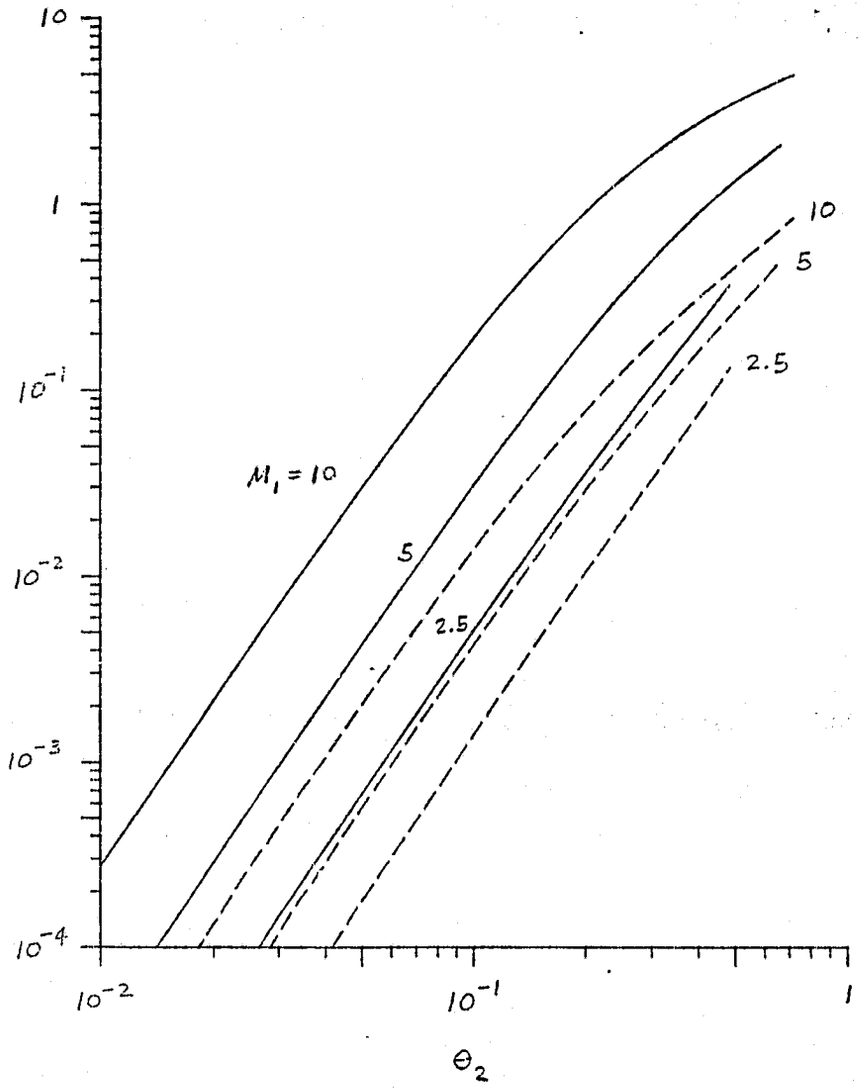

Fig 2

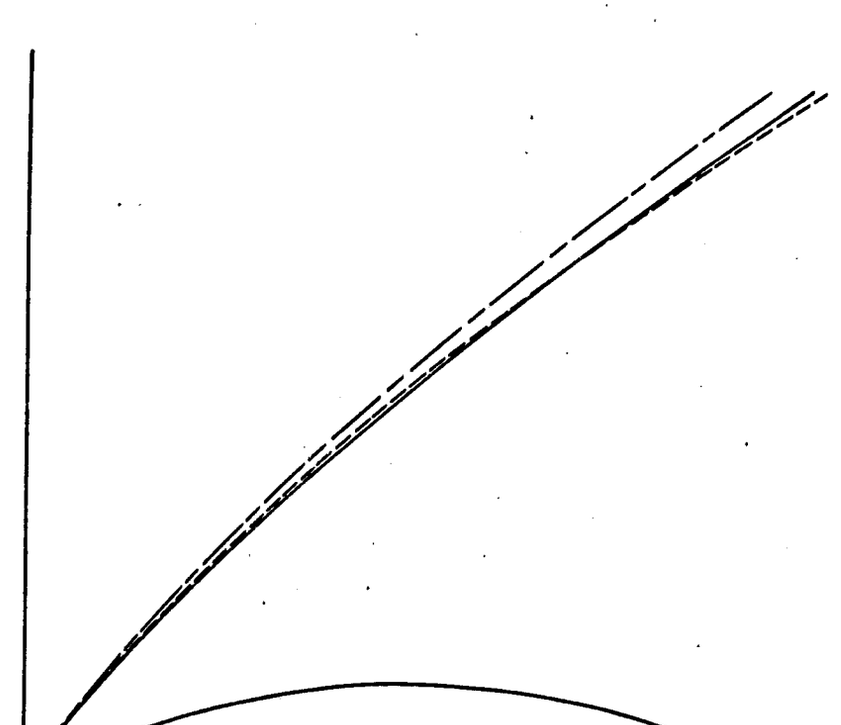

FIG 3

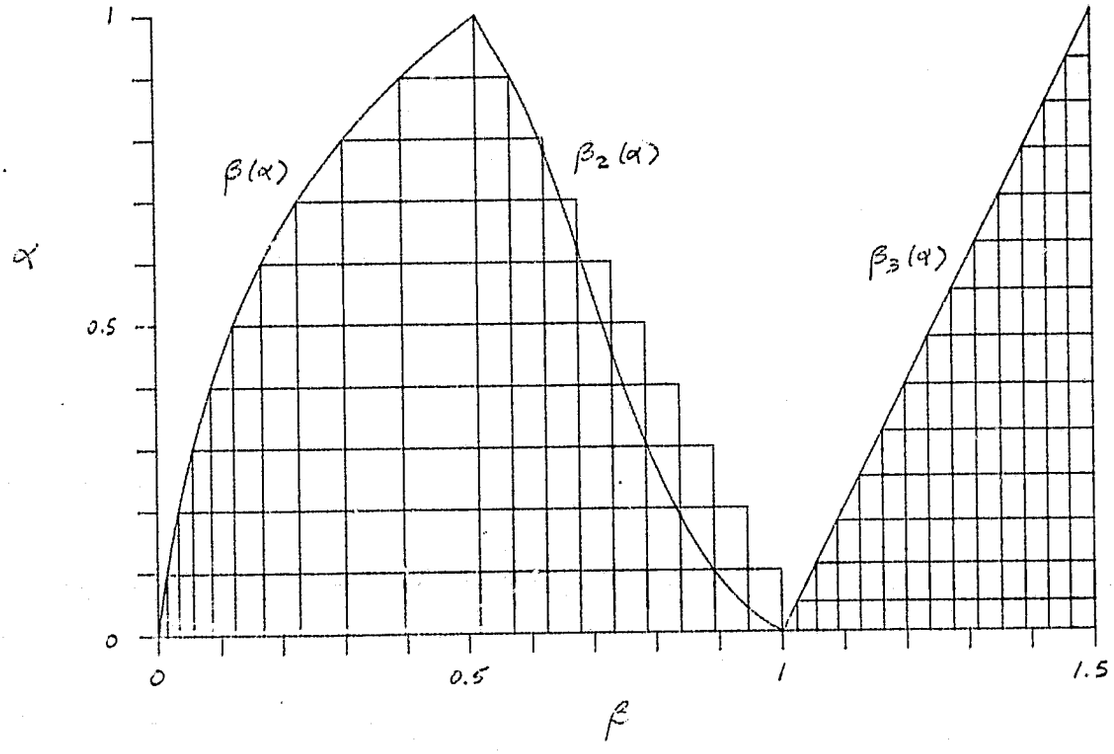

Fig 4

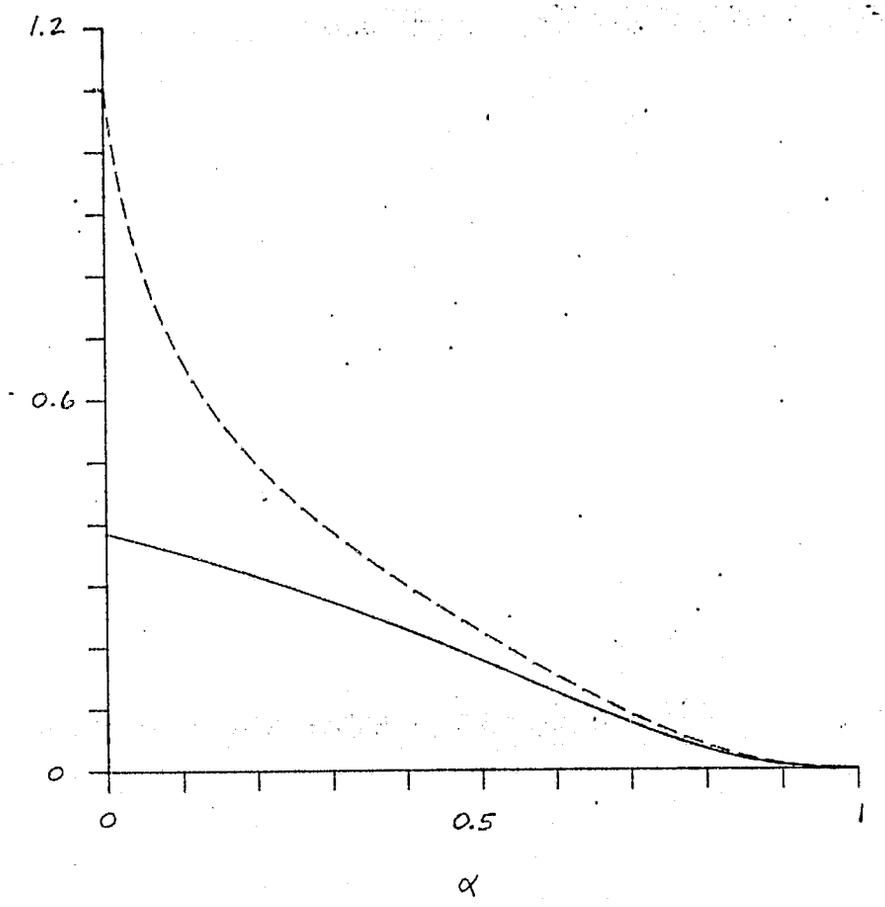

Fig 5

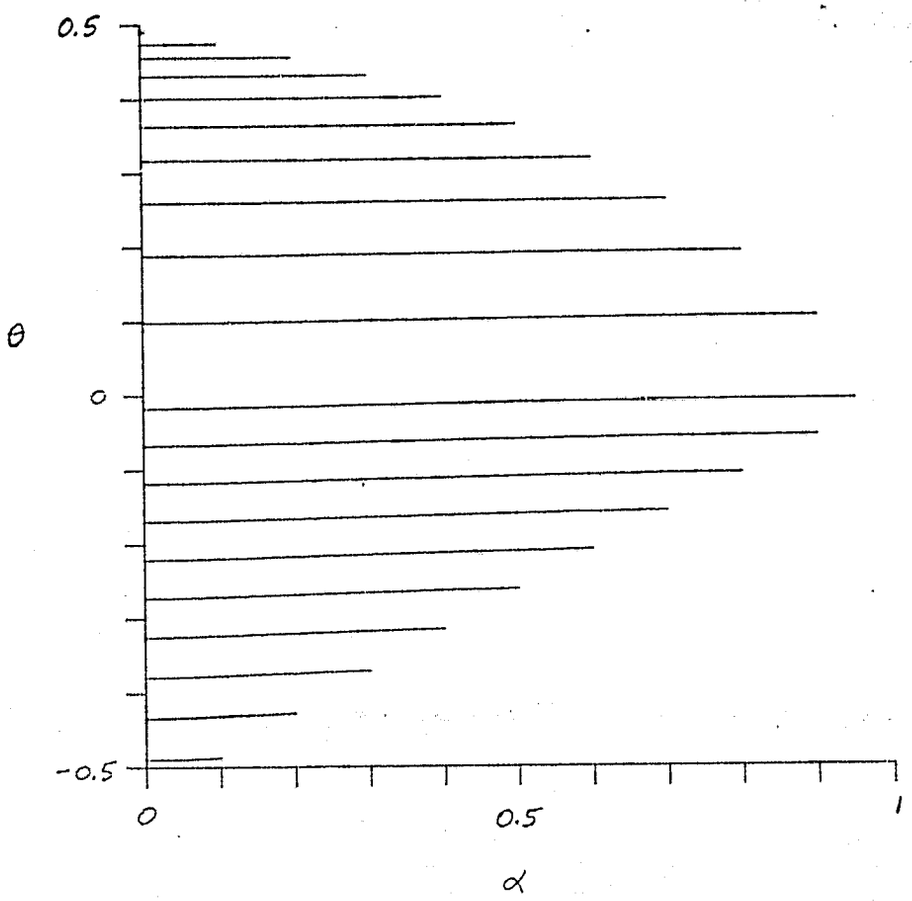

Fig 6

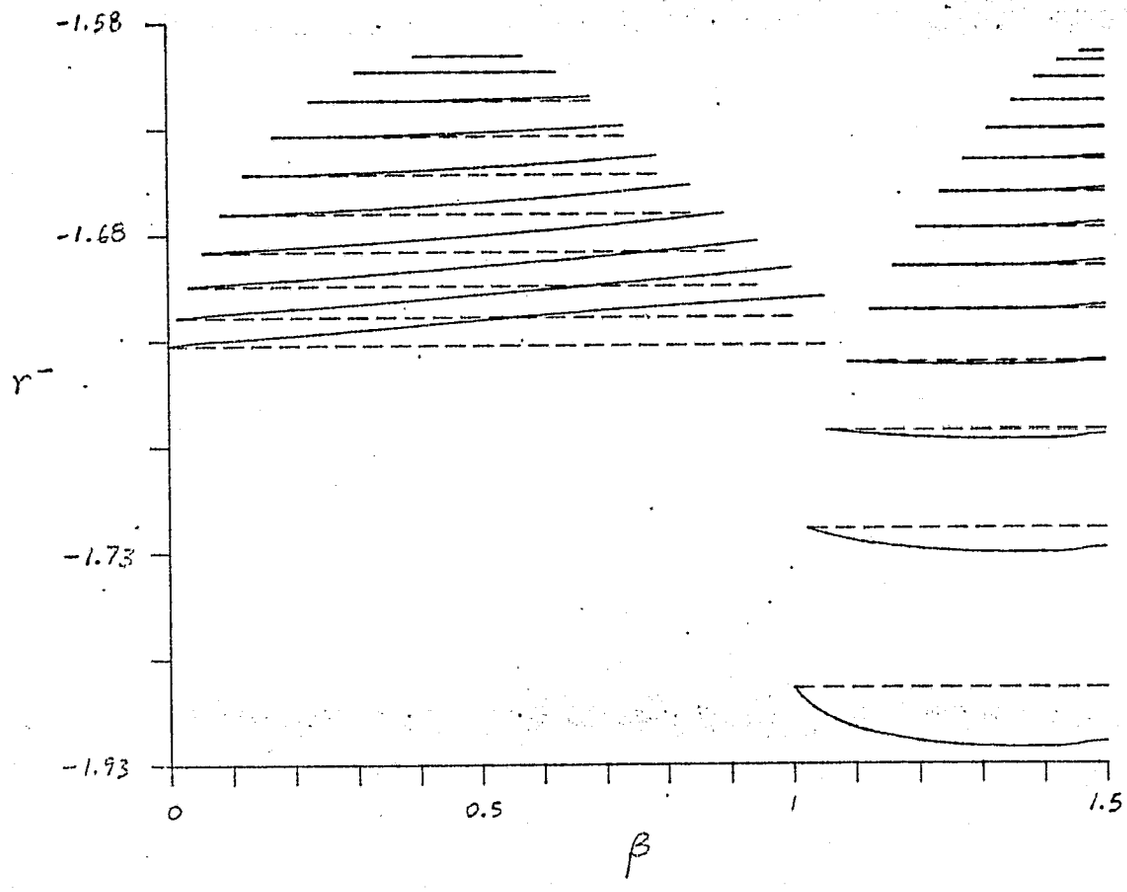

Fig 7

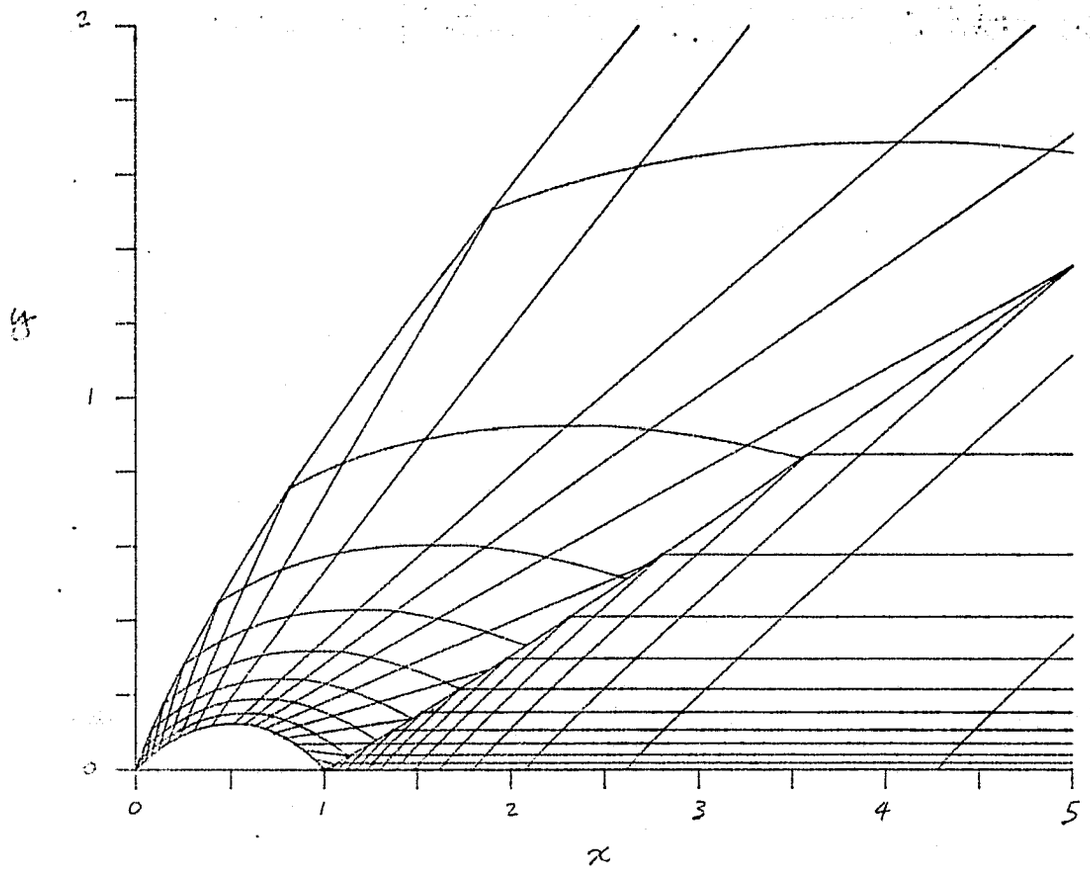

Fig 8

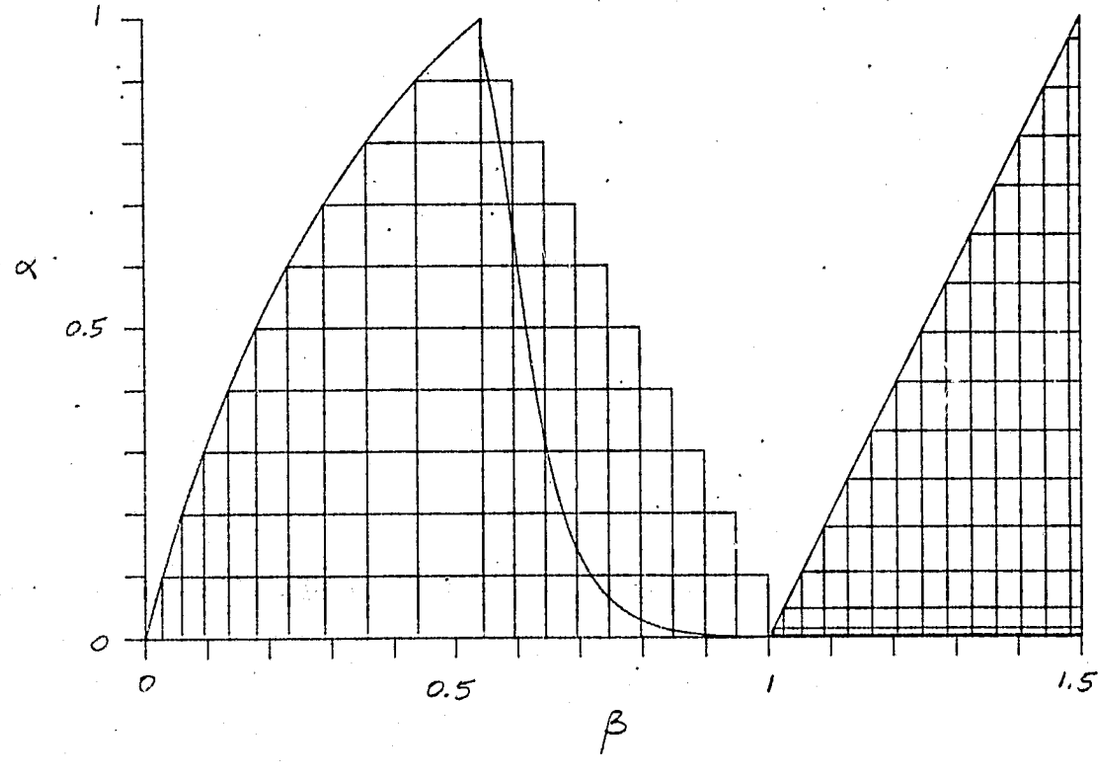

Fig 9

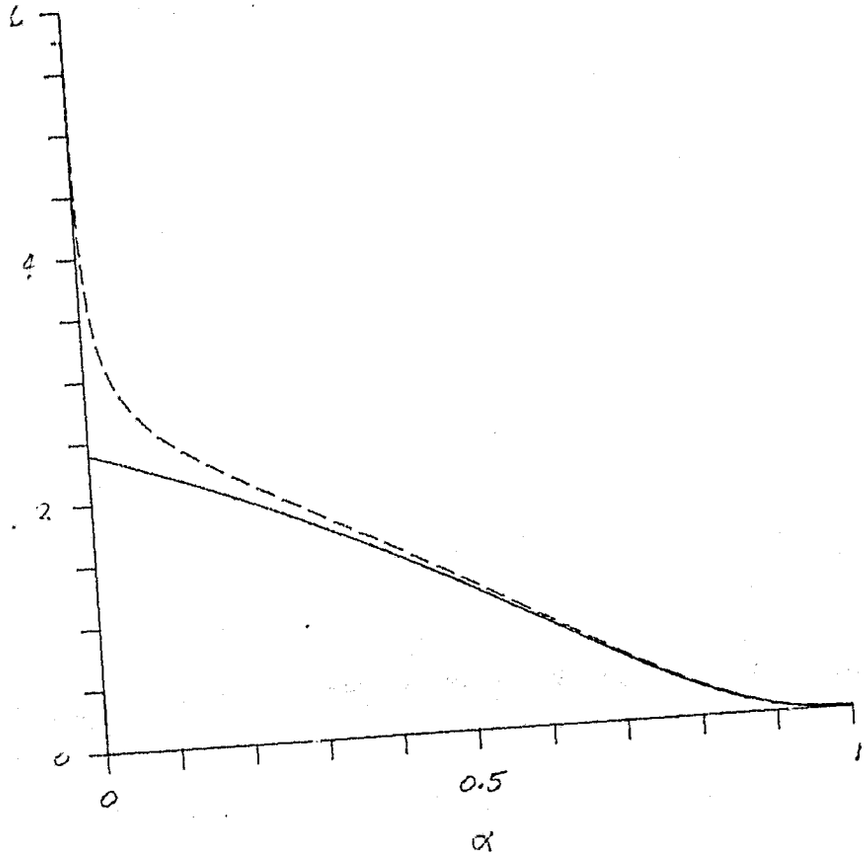

Fig 10

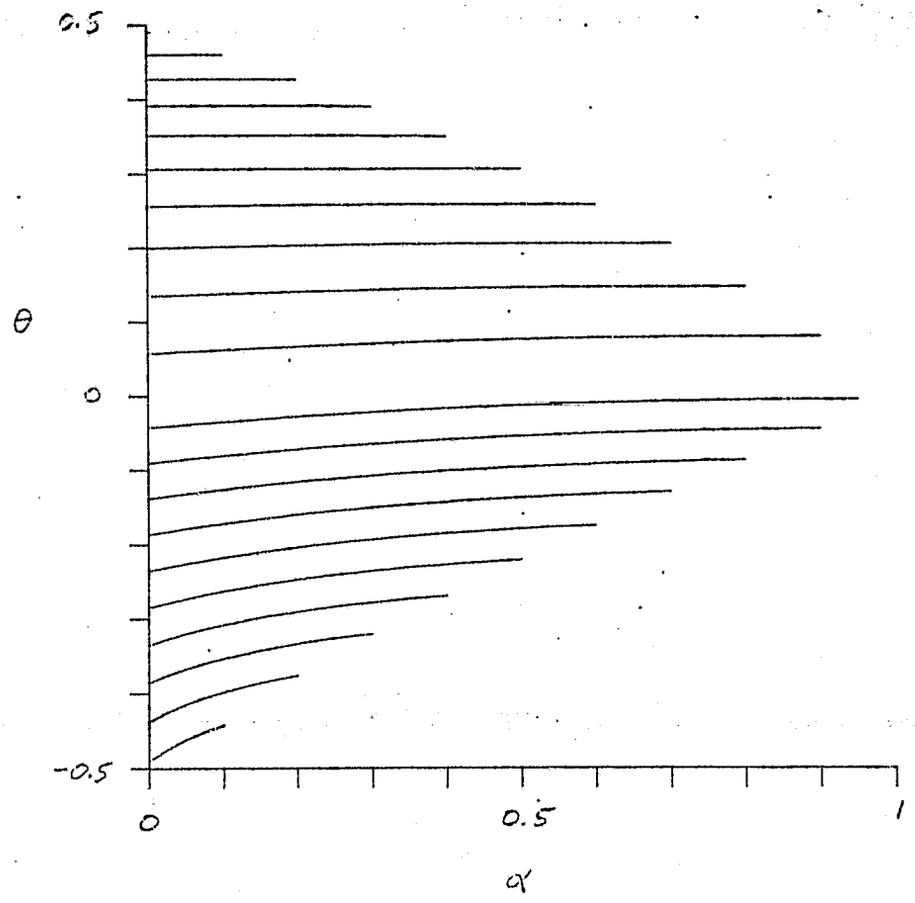

Fig 11

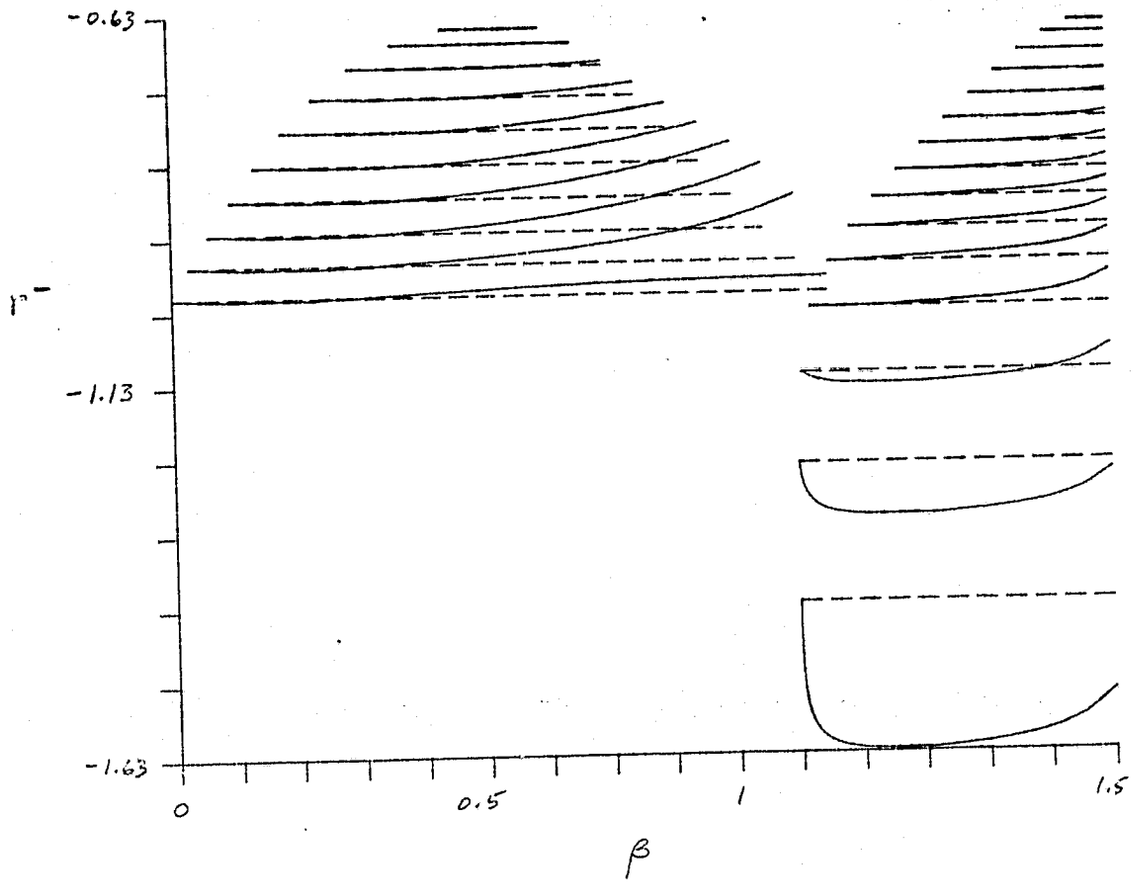

Fig 12

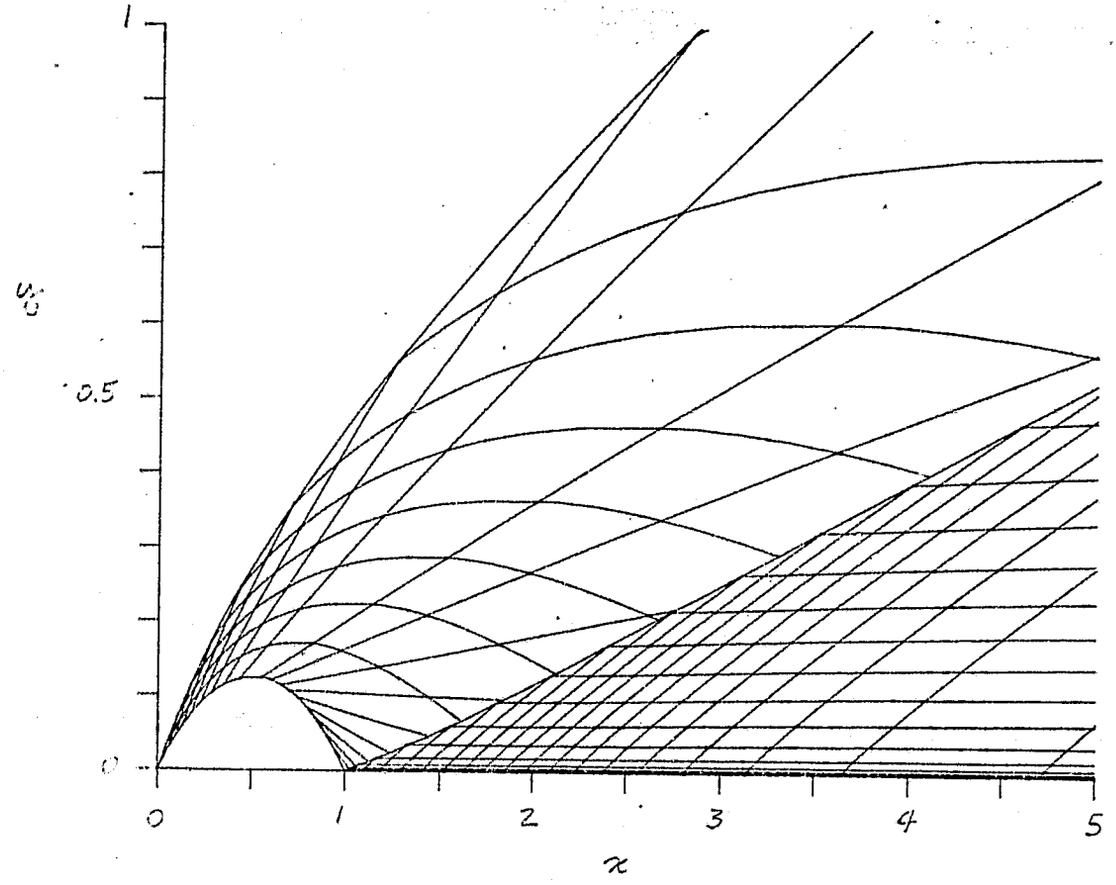

Fig 13

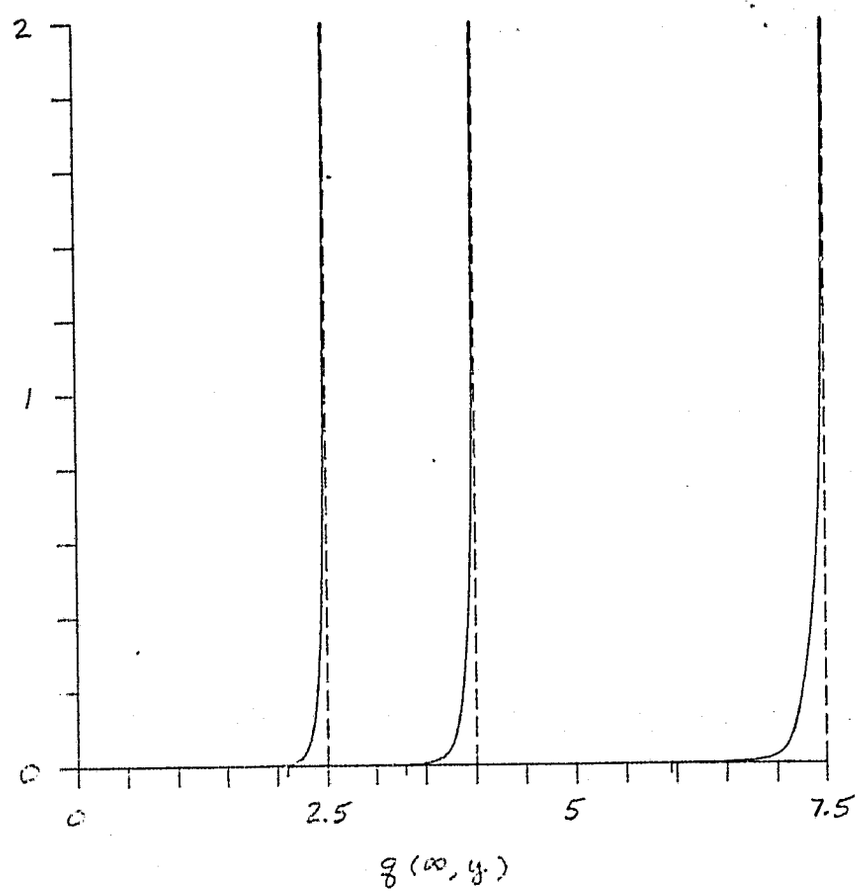

Fig 14

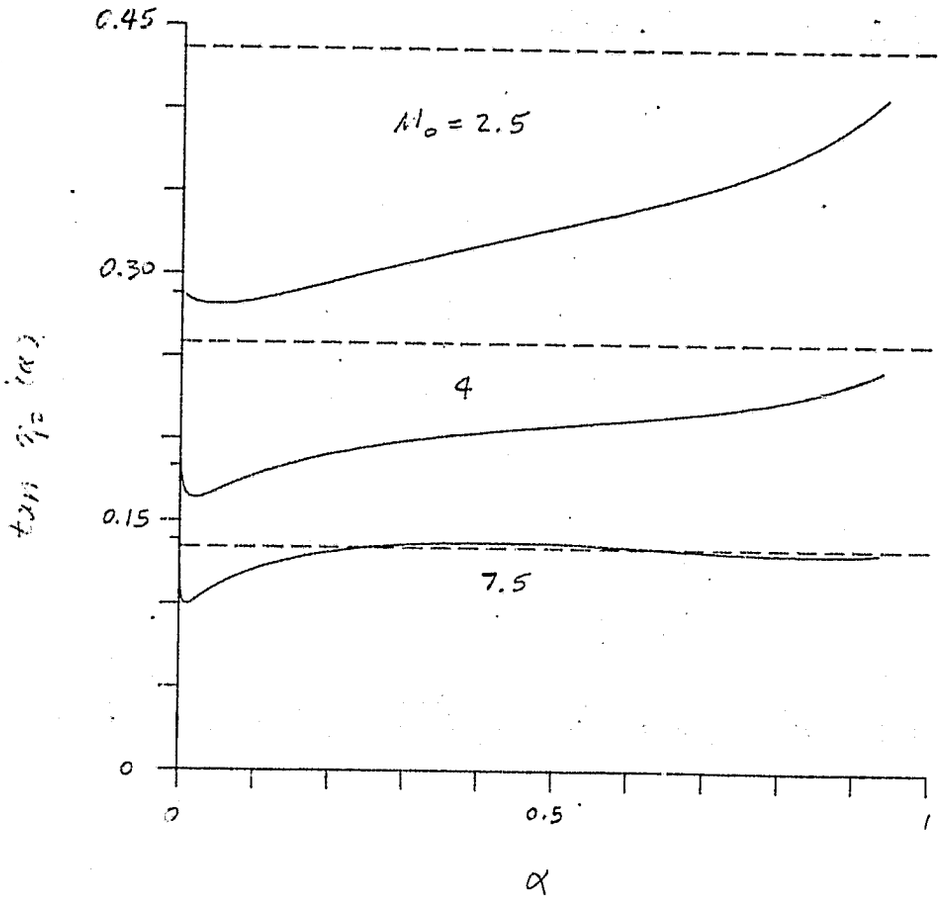

Fig 15

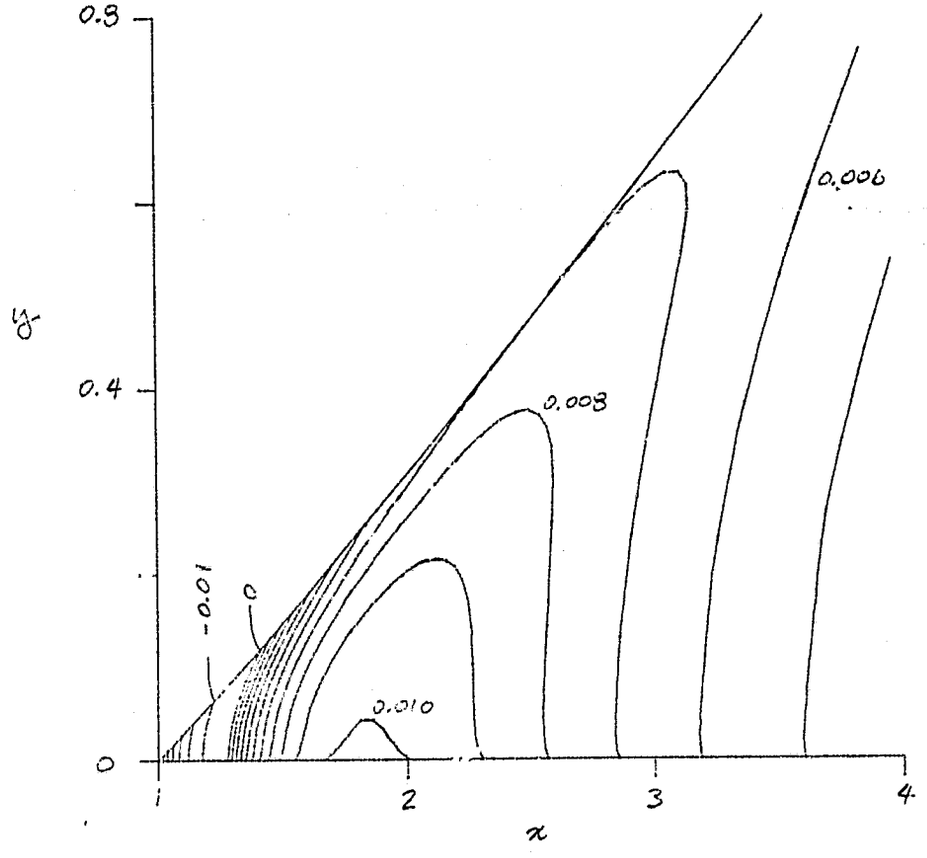

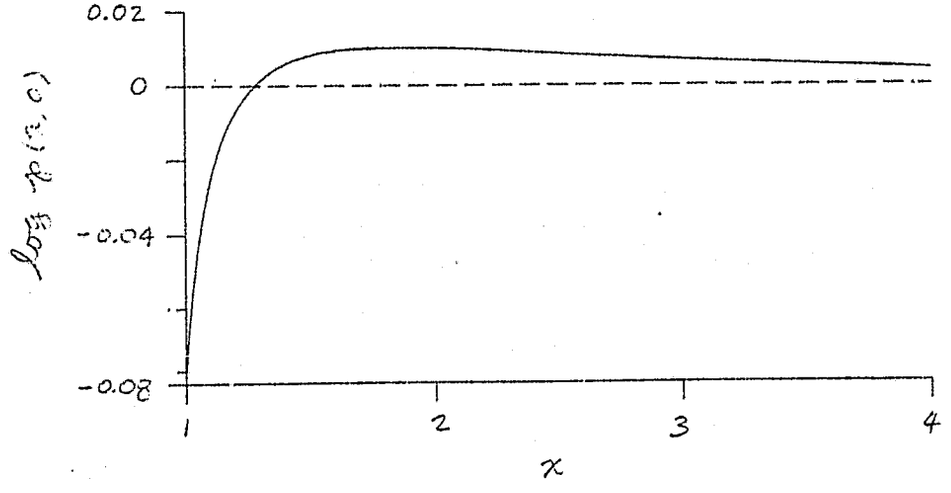

Fig 16

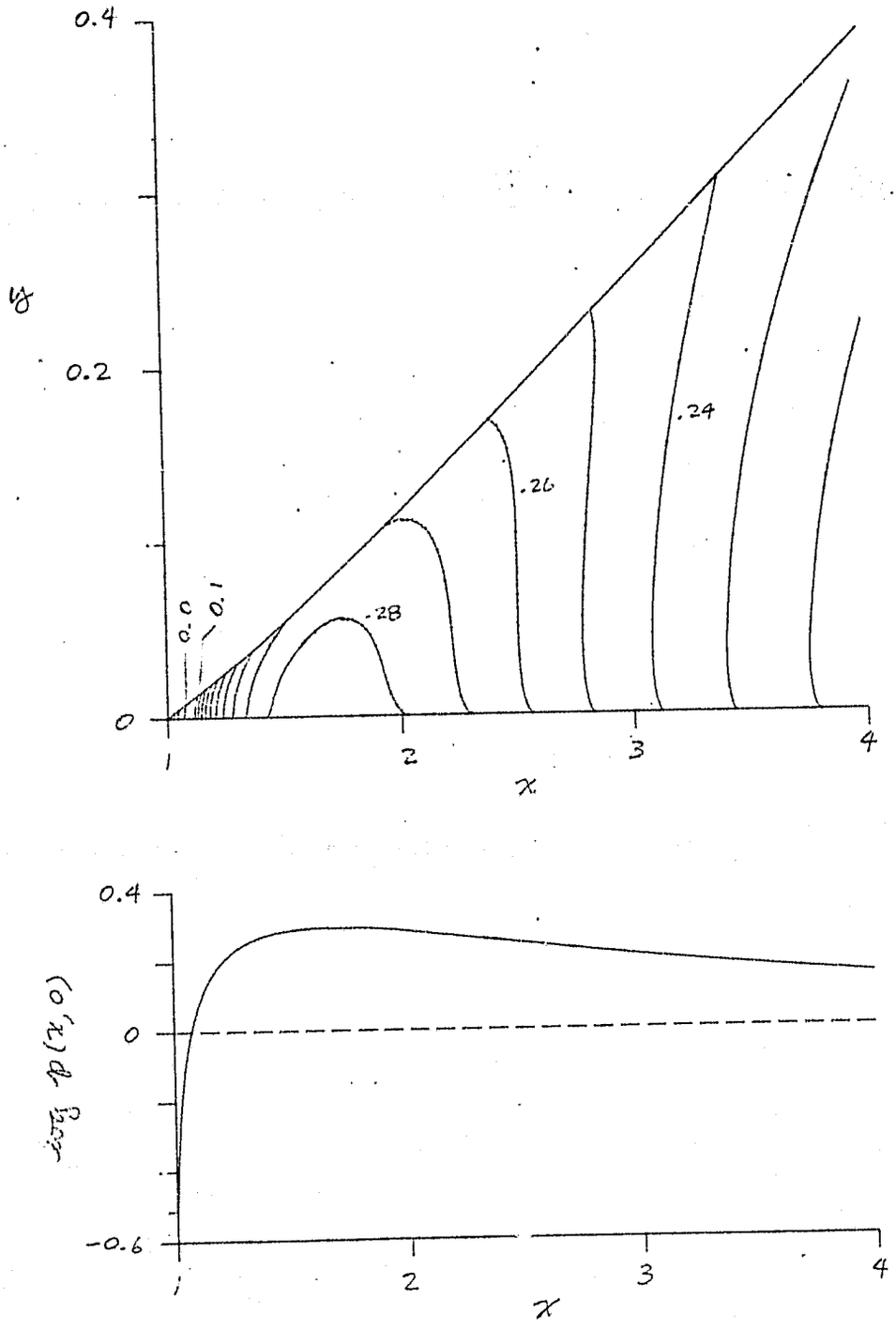

Fig 17